Canon

Medical Review

Celesteion

# Time-of-Flight Technology

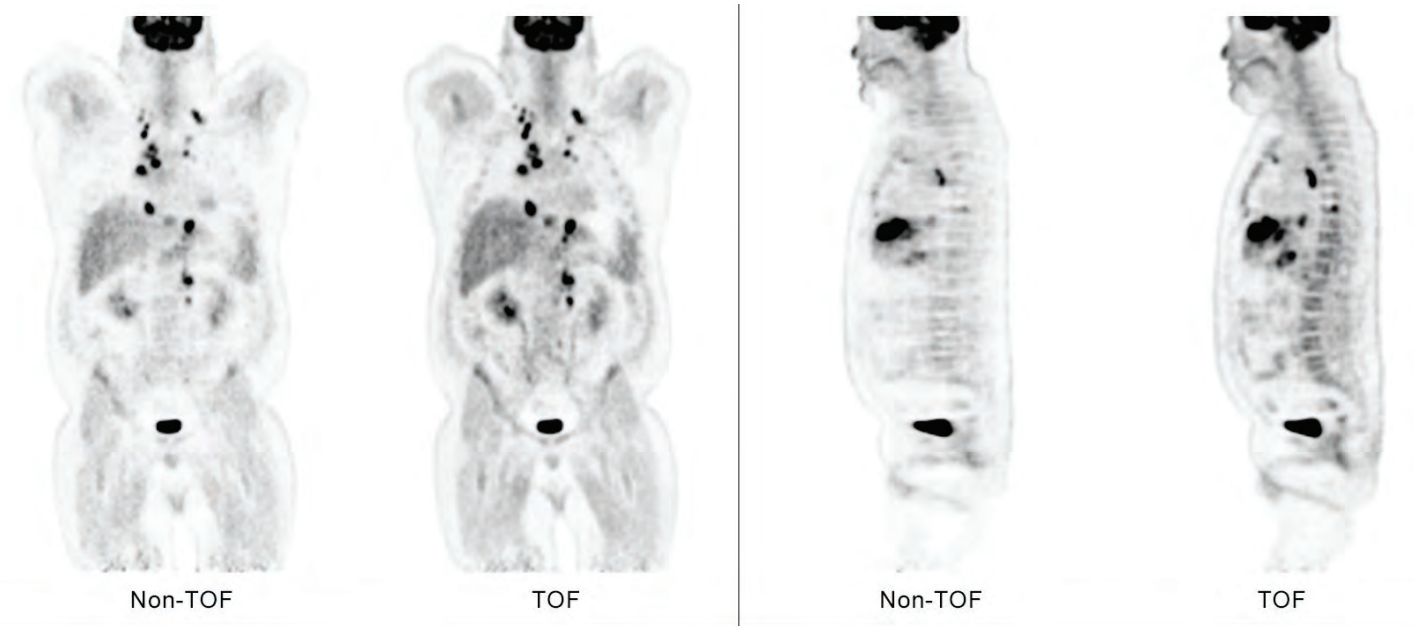


***Bing Bai, PhD***
*Clinical Sciences Manager, PET/CT*
*Canon Medical Systems*

## INTRODUCTION

Improving the care for every patient while providing a high standard care to the entire population of patients you treat is a goal of every provider of healthcare today. Providing quality and safer care is always weighed with reducing the total cost of that care and providing high end technology that can possibly help providers is the goal of Canon Medical Systems and the goal of Celesteion™ PET/CT.

Celesteion is designed with patients in mind. With the industry's largest bore of 90 cm (CT) and 88 cm (PET), a true scan field of view at 70 cm (CT and PET) and Time-of-Flight technology, Celesteion can enable facilities to improve care and maximize their investment.

Positron emission tomography (PET) is a widely used molecular imaging modality with a broad range of clinical applications in oncology, neurology and cardiology. Over the last two decades, tremendous advancements in instrumentation and data processing methods have greatly improved image quality. One of the latest technical developments is the evolution of time-of-flight (TOF) PET, where the difference between the arrival times at the detectors of the two photons is measured and used to help to identify the location of the radioisotope injected into the patient. By incorporating the TOF information in image reconstruction, the signal-to-noise ratio (SNR) and contrast recovery of the image can be substantially improved, especially for large patients.

Patients undergoing PET imaging receive radiopharmaceuticals labeled with positron-emitting isotope. A positron produced from radioactive decay travels a short distance before annihilating with an electron. The annihilation generates two 511 keV photons emitted in opposite directions. These photons are detected in the scanner and processed through electronics to check for various criteria such as if each photon has the right amount of energy (typically between 350-650 keV) and if the photons have arrived almost simultaneously (within 5-6 ns or less of each other). If all criteria are satisfied, then a coincidence event is recorded. Each coincidence event can be stored separately as is the case with "list-mode" data or alternatively, the total number of events detected at each detector pair can be stored. A mathematical

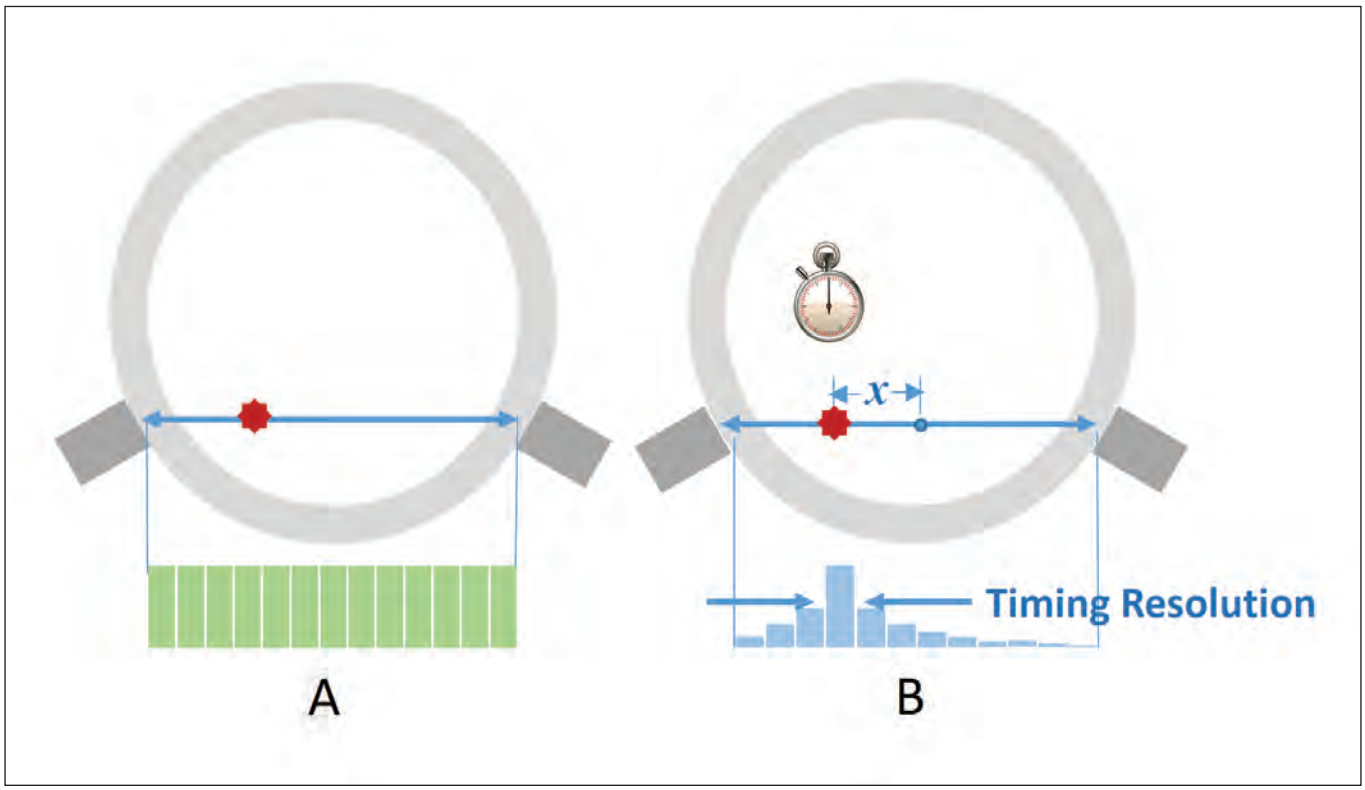


**Figure 1: Illustration of Conventional PET (A) and TOF PET (B).**

algorithm is then applied to reconstruct the distribution of the radiopharmaceuticals from the collected PET data.

Conventional PET only uses the total number of events between each detector pair for image reconstruction, as shown in Figure 1A. With TOF-PET, the difference between arrival times at the two detectors is measured and used to pinpoint the location of the source, as shown in Figure 1B. The distance between the source and the center of the line connecting the detector pair (called line of response, or LOR) x can be computed from the arrival time difference t as:

$$x = \frac{c}{2}t \quad (1)$$

where c is the speed of light.

Theoretically, if we could measure the arrival time difference t perfectly, then we could put each coincidence event back to the source location, and no tomographic reconstruction algorithm would be needed. However, even the fastest PET detector technology today can only achieve a timing resolution of about 400 picosecond, which results in a distance uncertainty of about 6 cm. The spatial resolution of clinical PET scanners is about 5 mm. Therefore, the effects of TOF on image resolution is negligible.

Improving lesion detection and accuracy is a key component to improved treatment planning with possible better outcomes when treating Oncology patients. The major advantage of TOF is the improvement in image SNR, which results in better lesion detection performance[1]. To understand the SNR benefit of TOF, let's assume an analytic reconstruction algorithm such as filtered backprojection (FBP) is applied to the data. In FBP, the projection data is filtered, then backprojected to image space. If we look at the LOR in Figure 1A, the value of each image pixel along the LOR is increased by an amount proportional to the number of events measured between the two detectors at the ends of the LOR. All the events recorded in the LOR contribute equally to all the pixels along the LOR and add noise to the pixels. With TOF, the contribution of each event to each pixel is weighted by the probability of the event occurred when the two photons are emitted from the pixel, as shown in Figure 1B. As a result, only the events near the pixel where it originated contribute to the pixel and add noise to it. Based on this analysis, we can derive the following SNR improvement factor using TOF information[2,3]:

$$\frac{SNR_{TOF}^2}{SNR_{Non-TOF}^2} = \frac{2D}{c\Delta t} \quad (2)$$

where D is the diameter of the subject being imaged and Δt is the timing resolution.

The above SNR gain factor was originally derived for the central pixel in a uniform disk source scanned using 2D PET and reconstructed using FBP. Later experiments on modern 3D PET scanners using iterative reconstruction algorithms show similar results for both phantom and clinical patient studies.[4–6] It has also been demonstrated that as randoms ratio increases (randoms are events detected when the two photons arrive at the detectors simultaneously are not related to each other, which happens more often when more radioactivity is injected), the SNR gain due to TOF also increases.[6] Furthermore, phantom studies suggest that TOF image quality with reduced counts (through less injected dose or shorter scan time) is equivalent to conventional non-TOF image.[4] Therefore, TOF technology can possibly reduce radiation dose, PET scan time and overall table time

| | NaI(Tl) | $BaF_2$ | BGO | LSO | LYSO |
|---|---|---|---|---|---|
| **Effective Z** | **51** | **54** | **74** | **66** | **60** |
| **Linear atten. coeff. ($cm^1$)** | **0.34** | **0.44** | **0.92** | **0.87** | **0.86** |
| **Density ($gm/cm^3$)** | **3.67** | **4.89** | **7.13** | **7.4** | **7.1** |
| **Light yield (% NaI(Tl))** | **100** | **5** | **15** | **75** | **80** |
| **Decay constant (ns)** | **230** | **0.8** | **300** | **40** | **41** |

**Table 1: Properties of some PET scintillators [7].**

for improved workflow and patient satisfaction during PET procedures. The dose (or time) reduction factor can be estimated using equation[2].

## CANON MEDICAL SYSTEM CELESTEION TOF PET TECHNOLOGY

### New Modular Detector Designed for TOF PET

Detector design is critical for PET. Scintillator is the material of choice for radiation detectors in PET. Table 1 lists the key properties of some PET scintillators.[7] The first generation of TOF PET scanners was built in the 1980s, using fast scintillators such as CsF and $BaF_2$.[8] Although timing resolution was sufficient, the low stopping power and weak light output made these scintillators less efficient. BGO detectors, which were developed shortly after, have much higher stopping power and acceptable light output and became the standard material for PET scanners for many years. Due to the long decay time and low light output, BGO is not useable for TOF PET and thus the development of TOF PET was paused. The discovery of Lutetium-based scintillators such as LSO and LYSO prompted the development of a new generation of PET scanners. These scintillators have short decay time and can be used for TOF PET. And unlike the TOF scintillators used in the 1980s, they have high stopping power and very good light output so the efficiency of the detector is not compromised.

In order to optimize the performance of the scanner for different clinical applications and patient populations, Canon Medical Systems' Celesteion PET/CT uses Lutetium-based scintillator and a new modular and scalable detector design.[9] Figure 2 shows a Celesteion PET detector module and two detector designs commonly used in commercial PET scanner. Each module is two-side buttable in the transaxial direction. Twelve photomultiplier tubes (PMTs) with two different sizes (25mm and 38mm) are arranged in a rectangular pattern. The scintillator area is divided into five overlap trigger zones. Each trigger zone has four PMTs and the neighboring zones share two PMTs.

The main features of Celesteion TOF PET detectors include:

#### *High Light Collection Efficiency*

The unique mixed-size PMT design of Celesteion PET module ensures high light collection efficiency, which is critical for excellent timing resolution. This is achieved by optimizing the geometric coverage ratio of the scintillator area by the

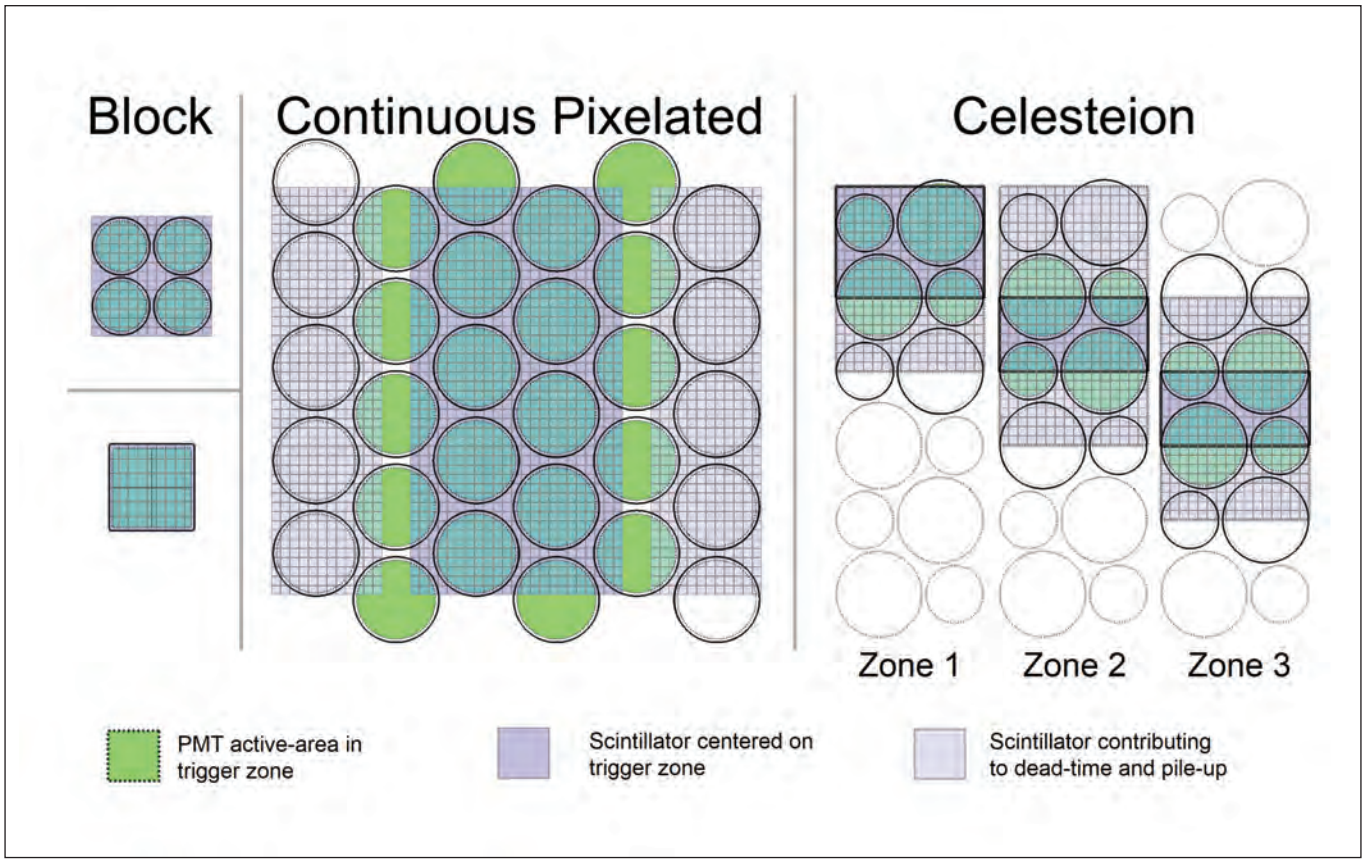


**Figure 2: Celesteion PET detector module and two PET detector designs commonly used for commercial PET scanners [9]**

active areas of the PMTs. Figure 3 shows the calculated geometric coverage ratio as a function of the size of the PMTs. By combining 25mm and 38mm PMTs, the Canon Medical System Celesteion achieves a geometric coverage ratio that is near optimal.

Detector crystals near the edge of PET detector modules have lower detection efficiency and light collection efficiency, deteriorating the performance. Celesteion PET detector has about 16% edge crystals, much less than what is typical for block detectors (30-50%).

Figure 4 shows the uniformity of light collection efficiency of a Celesteion PET module and a block detector module.[10] On average 94% of the light is collected by the four PMTs in each trigger zone. In contrast the block detector has many edge crystals which have lower efficiencies than those in the center of the block.

### *Excellent Count-Rate Performance*

Some PET studies require larger amounts of radioactivity to be injected into the patient. For example, in a stress-rest myocardial perfusion study 25-50 mCi of Rubidium-82 may be injected, which results in the very high count rate necessary for the exam.[11] As count rate increases, PET detector performance deteriorates due to deadtime and pile-up effect. The area of scintillator coupled to a single trigger zone determines the PET scanner performance

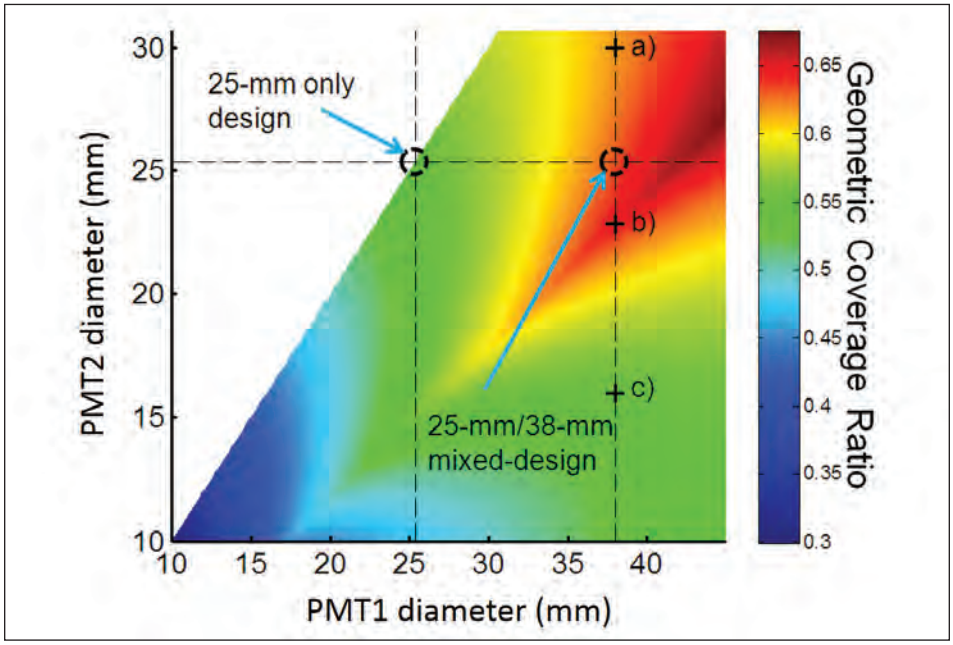


**Figure 3: Geometric coverage ratio as a function of PMT diameters. The 25/38 mm mixed-design is used in Celesteion, resulting in near optimal geometric coverage ratio [9].**

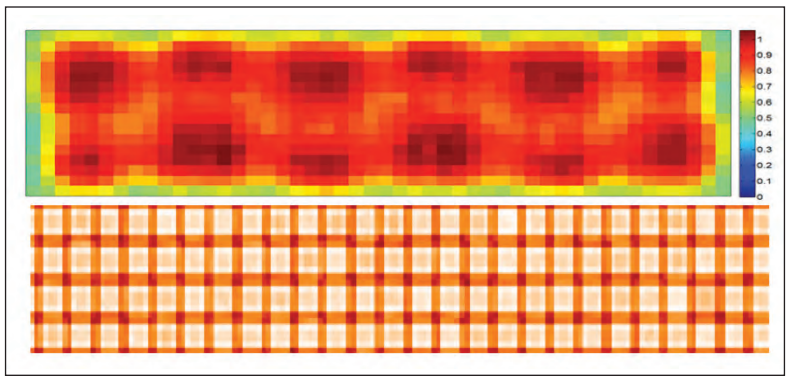

**Figure 4: Light collection efficiency of Celesteion detector module [9] and a block detector module [10]**

at high count rates. Smaller trigger areas will reduce the deadtime and pile-up effect.

### *Best In-Class Timing Resolution*

The combination of fast, bright Lutetium-based scintillator, fast PMTs and mixed-size, modulated detector design results in excellent timing resolution of Celesteion. The timing resolution of Celesteion was measured using two cylindrical phantoms filled with F18 solution and a Ge68 point source between the phantoms[9]. This experimental setup represents the situation encountered in the clinic, with large proportion of lower-energy scattered radiation. Timing resolution was measured as a function of system singles rate (singles counts all the individual photons detected in the scanner). Figure 5 shows the result. As expected, the timing resolution of Celesteion PET detectors gets slightly worse as singles rate increases. Nevertheless the modulated detector design of the Celesteion outperforms block detectors and continuous pixelated detectors at all singles rates. Also the timing resolution of continuous pixelated detectors gets worse at a faster rate when the singles rate increases as expected.

## EVALUATION OF TOF BENEFITS

To demonstrate the improvement to image quality using TOF, we scanned a 35cm diameter cylindrical phantom. Twelve spherical inserts were attached to the removable cap in two radii. Six spheres with inner diameters between 10 mm and 37 mm were inserted in the inner radius (about 6 cm from the sphere centers to the center of the phantom). Another six spheres with inner diameters of between 3.95 mm and 13 mm were inserted in the outer radius (about 10 cm from the sphere center to the center of the phantom). $^{18}$F-FDG solutions were injected into the background and spheres. The phantom was positioned such that the center of the spheres were located in the axial center of the scanner FOV. We scanned the phantom for 2 minutes and 10 minutes respectively. The background activity concentration was 4.6 kBq/cc at the beginning of the scan, and the sphere-to-background concentration ratio was 8.4.

We reconstructed the data using a 3D listmode OSEM algorithm with and without TOF. A new area-simulating-volume (ASV) projector has been developed for Celesteion, which accurately models the PET system and is very fast to compute.[15] Twenty subsets were used for both TOF and

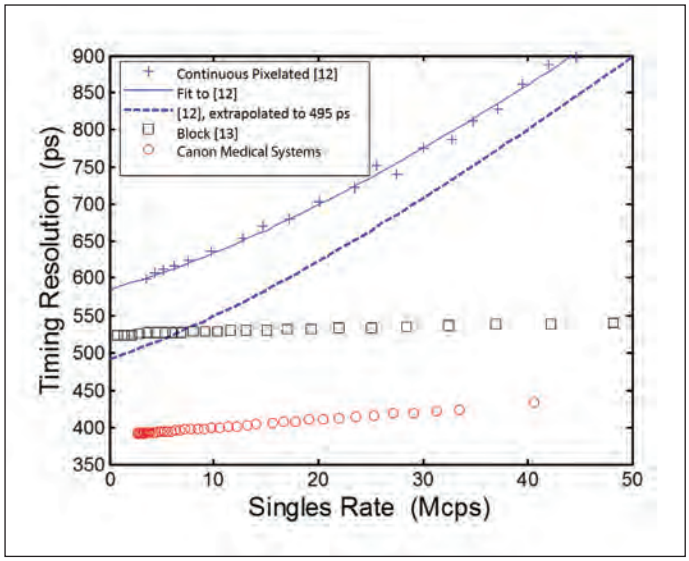


**Figure 5: Timing resolution as a function of system singles rate. The blue symbols (+) and black symbols (squares) were digitized from [12] and [13], respectively. The blue dashed line is extrapolated based on timing resolution of 495 ps measured on newer scanners [14].**

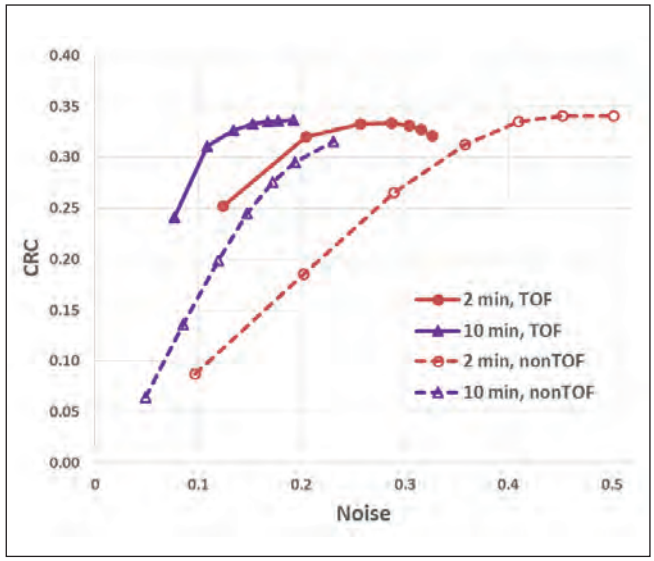


**Figure 6: Contrast vs. noise plot for the 10 mm diameter sphere in the 35 cm diameter cylindrical phantom scanned on Celesteion.**

non-TOF reconstruction. A Gaussian filter with 6mm FWHM was applied after the image was reconstructed. We drew a 10 mm diameter spherical region of interest (ROI) on the 10 mm sphere in the inner circle and measured the mean $\mu_H$. A 30 mm diameter spherical ROI was drawn in the central background area of the phantom, at least 25 mm away from all the spheres. The mean $\mu_B$ and standard deviation $\sigma_B$ of the background ROI were measured. The contrast recovery coefficient (CRC) and noise were given by:

$$CRC = \frac{(\mu_H - \mu_B)/\mu_B}{C} \quad (3)$$

$$Noise = \frac{\sigma_B}{\mu_B} \quad (4)$$

Figure 6 shows the CRC vs. noise measurements. First, we observe that the TOF reconstruction converges faster. After 3 iterations, TOF image is very close to the peak CRC value. With non-TOF, 5-8 iterations are necessary to achieve near peak CRC. Second, we note that the 2 minute TOF curve is much better than the 2 minute non-TOF curve, and even slightly better than the 10 minute non-TOF curve (higher CRC at the same noise level, or less noise with the same CRC). This shows that the quality of the 2 minute TOF image is slightly better than that of the 10 minute non-TOF image. Using the simple TOF gain equation (2) and the measured TOF timing resolution of 420 ps, we can calculate the time reduction factor using TOF (TOF gain) as:

$$TOF\ gain = \frac{2D}{c\Delta t} = \frac{2 \times 35(cm)}{0.03(\frac{cm}{ps}) \times 420(ps)} = 5.6 \quad (5)$$

The CRC vs. noise curves in Figure 6 shows that the TOF gain is slightly better than 5, which is consistent with the estimation using equation (2).

From Figure 6 we can see that the TOF image from 2 minute data reconstructed using 2 iterations of OSEM has similar CRC and noise as non-TOF image from 10 minute data reconstructed using 8 iterations of OSEM. Figure 7 shows these two images. Similar image quality is seen in both images, while the acquisition time is different by a factor of five.

## CONCLUSIONS

It has been demonstrated in the literature that TOF PET can improve SNR and contrast recovery of image, compared to the conventional, non-TOF PET technology. As a result, PET studies using TOF technology can be done with less scan time. The TOF gain gets larger as the timing resolution gets better or when the patient is bigger. Using innovative technologies such as the modular PET detector, Celesteion PET/CT has achieved excellent timing resolution and image quality. Phantom study suggests that for a 35 cm diameter subject, TOF may reduce the dose or time by a factor of five, without sacrificing the image quality.

Improving the quality of care with technology like a large bore, a large field of view and 3D listmode TOF reconstruction. Celesteion can provide improved accuracy and possibility a safer, faster and overall a better patient experience.

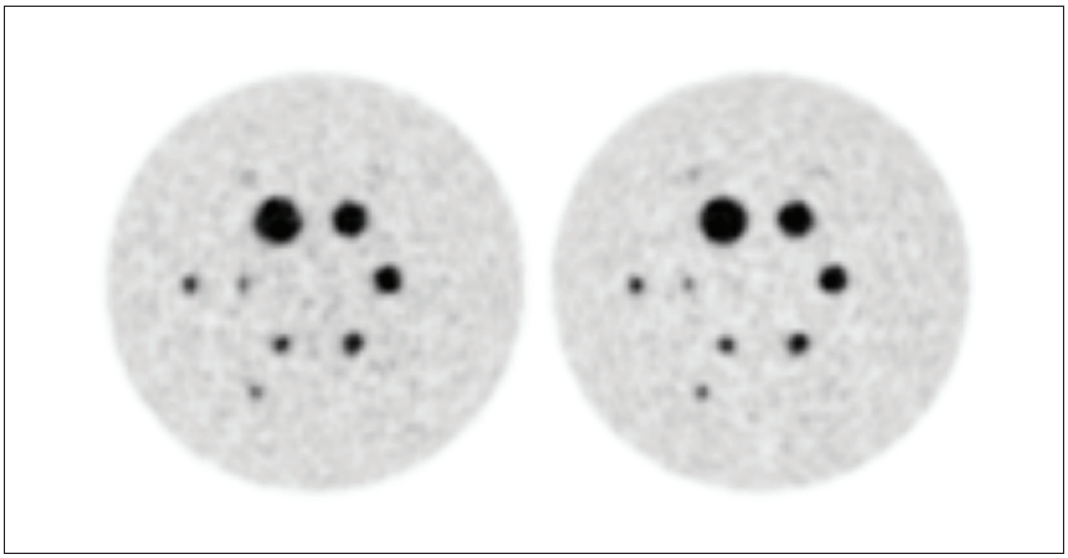

**Figure 7: TOF image from 2 minute scan (left) and non-TOF image from 10 minute scan (right). The TOF image was reconstructed using 2 iterations of OSEM, while the non-TOF image was reconstructed using 8 iterations of OSEM. Both with 20 subsets and 6 mm Gaussian post filter.**

## REFERENCES


1. T. H. Farquhar, J. Llacer, J. Sayre, Y.-C. Tai, and E. J. Hoffman, "ROC and LROC analyses of the effects of lesion contrast, size, and signal-to-noise ratio on detectability in PET images," J. Nucl. Med., vol. 41, no. 4, p. 745, 2000.

2. T. F. Budinger, "Time-of-flight positron emission tomography: status relative to conventional PET," J. Nucl. Med., vol. 24, no. 1, pp. 73–78, 1983.

3. W. Moses, "Time of flight in PET revisited," Nucl. Sci. IEEE Trans. On, vol. 50, no. 5, pp. 1325–1330, 2003.

4. S. Surti, S. Karp, L. M. Popescu, E. Daube-Witherspoon, and M. Werner, "Investigation of time-of-flight benefit for fully 3-DPET," IEEE Trans Med Imaging, vol. 25, no. 5, pp. 529–538, 2006.

5. C. Lois, B. W. Jakoby, M. J. Long, K. F. Hubner, D. W. Barker, M. E. Casey, M. Conti, V. Y. Panin, D. J. Kadrmas, and D. W. Townsend, "An assessment of the impact of incorporating time-of-flight information into clinical PET/CT imaging," J. Nucl. Med., vol. 51, no. 2, pp. 237–245, 2010.

6. G. Mettivier, V. Tabacchini, M. Conti, and P. Russo, "Signal-to-noise gain at variable randoms ratio in TOF PET," Nucl. Sci. IEEE Trans. On, vol. 59, no. 5, pp. 1948–1957, 2012.

7. T. K. Lewellen, "Recent developments in PET detector technology," Phys. Med. Biol., vol. 53, no. 17, p. R287, 2008.

8. M. Conti, "State of the art and challenges of time-of-flight PET," Phys. Med., vol. 25, no. 1, pp. 1–11, 2009.

9. K. C. Burr, G.-C. Wang, H. Du, G. Mann, K. Balakrishnan, J. Wang, X. Li, C. Rollet, E. Kundro, and M. Buhin, "A new modular and scalable detector for a Time-of-Flight PET scanner," presented at the Nuclear Science Symposium and Medical Imaging Conference (NSS/MIC), 2012 IEEE, 2012, pp. 2830–2834.

10. J. J. Williams, D. L. McDaniel, C. L. Kim, and L. J. West, "Detector characterization of discovery ST whole-body PET scanner," presented at the Nuclear Science Symposium Conference Record, 2003 IEEE, 2003, vol. 2, pp. 717–721.

11. R. Nakazato, D. S. Berman, E. Alexanderson, and P. Slomka, "Myocardial perfusion imaging with PET," Imaging Med., vol. 5, no. 1, pp. 35–46, 2013.

12. S. Surti, A. Kuhn, M. E. Werner, A. E. Perkins, J. Kolthammer, and J. S. Karp, "Performance of Philips Gemini TF PET/CT scanner with special consideration for its time-of-flight imaging capabilities," J. Nucl. Med., vol. 48, no. 3, pp. 471–480, 2007.

13. B. Jakoby, Y. Bercier, M. Conti, M. Casey, T. Gremillion, C. Hayden, B. Bendriem, and D. Townsend, "Performance investigation of a time-of-flight PET/CT scanner," presented at the Nuclear Science Symposium Conference Record, 2008. NSS'08. IEEE, 2008, pp. 3738–3743.

14. A. Perkins, "Astonish TF: Technical overview of Philips time-of-flight PET design and its clinical behavior." Philips Healthcare.

15. H. Ye, X. Niu, and W. Wang, "Improved list-mode reconstruction with an Area-Simulating-Volume projector in 3D PET," presented at the Nuclear Science Symposium and Medical Imaging Conference (NSS/MIC), 2012 IEEE, 2012, pp. 3311–3314.





Canon

CANON MEDICAL SYSTEMS USA, INC.

https://us.medical.canon

2441 Michelle Drive, Tustin CA 92780 | 800.421.1968





CTWP12776US MCAMR0134EBA


Made For life